JOURNAL OF SOLID STATE CHEMISTRY 79, 112–118 (1989)

# Identification of Lithium Atoms in Solid Oxides: A High-Resolution Electron Microscopic Study of $LiMn_2O_4$

D. TANG AND D. A. JEFFERSON

*Department of Physical Chemistry, University of Cambridge, Lensfield Road, Cambridge CB2 1EP, United Kingdom*

I. J. PICKERING, A. HARRIMAN, AND J. M. THOMAS

*Davy-Faraday Research Laboratory, The Royal Institution of Great Britain, 21, Albemarle Street, London W1X 4BS, United Kingdom*

AND R. D. BRYDSON

*Department of Physical Chemistry, University of Cambridge, Lensfield Road, Cambridge CB2 1EP, United Kingdom*

Received September 1, 1988

High-resolution electron microscopic (HREM) images of $LiMn_2O_4$ and $\lambda$-$MnO_2$ have been investigated both experimentally and theoretically. Comparisons of computer-simulated and observed HREM images indicate that the lithium atoms present in $LiMn_2O_4$ can, under certain conditions of specimen thickness and objective lens defocus, produce sufficient contrast to be identified. 

## Introduction

Under general conditions, the scattering of electrons from light atoms such as lithium gives insufficient contrast in a HREM image for these to be observed, unless all the other atoms in the structure are of similarly low atomic number. As a result, information concerning the location of lithium atoms is not normally obtainable from HREM images. However, earlier studies indicated (*1*) that, under special conditions of objective lens defocus and specimen thickness, the contrast of light atoms may actually be *enhanced* and contrast effects arising from their presence, such as the local reduction in symmetry observed when lithium is incorporated into the N–$Nb_2O_5$ structure (*2*), may consequently be made visible. In particular, in the case of $Li_2Ti_3O_7$ (*3*) theoretical studies of the image contrast both with and without the lithium atoms suggest that, under special conditions, the presence of these atoms modifies the image contrast to an appreciable extent.

As predicted by the "*pseudo weak phase object*" approximation (*1*), the contribution to the image contrast from a light element will increase relatively with crystal thickness, whereas for heavier atoms, the

0022-4596/89 $3.00

contrast will decrease and may even reverse its sign in sufficiently thick crystals. Recording images from thicker regions of crystals will therefore aid the detection of contrast effects arising from light atoms, but this has to be balanced against complications in the interpretation of this contrast which can arise at such thickness values when the pseudo-weak phase object approximation may cease to be valid. Consequently, only a full consideration of all the factors affecting the image, including multiple scattering and inelastic scattering, will enable valid predictions of the contrast effects to be made.

In the study described here, we compare experimental and simulated images of $LiMn_2O_4$ and $\lambda$-$MnO_2$, which differ only in the presence of lithium in the tunnel sites common to both structures. Full simulations using the multislice method (*4*) with allowance for factors such as absorption and the subsequent *elastic* scattering of initially *inelastically* scattered electrons (*5*) are described, and the results are compared with experimentally obtained HREM images of both materials.

## Experimental

$LiMn_2O_4$ was synthesized according to the method of Wickman and Croft (*6*), stoichiometric amounts of $Mn_2O_3$ and $Li_2CO_3$ being ground together and heated in air at 750°C for 30 hr, the specimens being removed from the furnace on two occasions during the heat treatment for further grinding to ensure intimate mixing. $\lambda$-$MnO_2$ was prepared from $LiMn_2O_4$ according to the method of Hunter (*7*), the latter compound being stirred in a solution of strong acid (ca. 2.5 *M*) for 13 hr to remove the lithium, followed by drying in air for 4 hr at 90°C.

Finely ground samples of both materials were deposited onto copper grids coated with holely carbon films from acetone suspension and examined at high resolution in a specially modified JOEL JEM-200CX electron microscope (*8*) with an *interpretable point resolution* (*9*) of approximately 1.95 A. Images were recorded at magnifications of ca. 450,000 and 700,000× in the [110] orientation for both materials, care being taken to minimize the effects of incident beam illumination (*10*), and residual astigmatism was corrected by observing the granularity of the amorphous carbon support film. Electron energy loss spectra (EELS) were recorded with a Gatan 607 spectrometer interfaced to a Canberra Series 80 multichannel analyzer.

Image simulations were performed using the multislice method (*4*) with programs specially modified for the inclusion of image components arising from elastic scattering of electrons scattered initially at a longer wavelength, this being taken account of by averaging over images at different defocus positions rather than reworking the calculations for slightly different wavelengths. Focal spread was incorporated also by image averaging, and as this was found to be the factor determining the absolute resolution limits of the experimental images, the effects of beam divergence were neglected. EELS spectra were deconvoluted to remove multiple inelastic scattering using the Fourier-log method described by Williams, Egerton, and Sparrow (*11*). The deconvolution procedure produces the spectrum that would be obtained from a very thin sample such as that employed in HREM imaging (ca. 10 nm). Consequently, from the plasmon peak intensities in this deconvoluted spectrum some estimate of the bulk transmission coefficient may be made.

## Discussion

The structures of both $LiMn_2O_4$ and $\lambda$-$MnO_2$ are cubic with unit cell dimensions of 8.24 and 8.03 Å, respectively (*7*). Figure 1 shows a schematic projection of the former

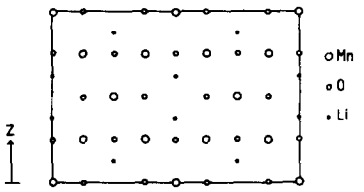


FIG. 1. Schematic representation of the structure of $LiMn_2O_4$ projected along [110]. Manganese atoms on the planes at $z = 0$ and $x = \frac{1}{2}$ project on top of one another and will therefore appear as atoms of double weight in this particular orientation.

structure down the [110] axis, where it is evident that in this projection the atoms are aligned into columns parallel to the projection axis, ideal for a HREM investigation, but unfortunately in this projection the separation of the lithium atoms and their nearest-neighboring oxygens is approximately 0.08 nm, well beyond the microscope resolution limit, such that any contrast effects due to their presence, if observed, will only be manifest in an alteration of the contrast of the neighboring oxygen atoms. All the columns of manganese atoms in this projection are not identical, inasmuch as those atoms lying in planes at $z = 0$ and $z = \frac{1}{2}$ project on top of one another, thus having apparently double the weight of those in the planes at $z = \frac{1}{4}$ and $z = \frac{3}{4}$. In terms of potential density, therefore, there are four different atomic columns in this projection, the two types of manganese columns, those of oxygen, and those of lithium atoms. The structure of $\lambda$-$MnO_2$ is virtually identical to that of $LiMn_2O_4$ except that the lithium atoms are omitted, with the result that in this projection there are clear channels in the structure parallel to the projection axis.

Figure 2 shows simulated images of both $LiMn_2O_4$ and $\lambda$-$MnO_2$ calculated at three different crystal thicknesses for a defocus slightly beyond the optimum or "Scherzer" position (*12*). Where the simulated specimen is thin, the predicted images for both structures are very similar, with large white dots present at the positions of the channel centers (Figs. 2a and 2d) and although the shapes of these white dots are not identical, the differences between them would almost certainly be lost in the "noise" of an experimental image. For greater crystal thicknesses, however, the differences between the two sets of images become more pronounced, with these white dots, although contracting in both cases, doing so in different ways. In the simulation of the $LiMn_2O_4$ images at 40 Å thickness the original white dot splits into two smaller ones, as shown in Fig. 2b, whereas for the $\lambda$-$MnO_2$ structure (Fig. 2e) the white dots merely contract isotropically, and in addition the decrease in the overall contrast of the dots is much less marked in the image of the former structure, in accordance with the principle that the *relative* scattering of the light atoms becomes more prominent with increasing specimen thickness. Because the lithium–oxygen distance in projection is beyond the resolution limit of the microscope, there is no dark dot in the image corresponding to the exact location of a lithium atom, but rather a dark minimum of intensity at a position midway between a pair of these atoms. As the crystal thickness in-

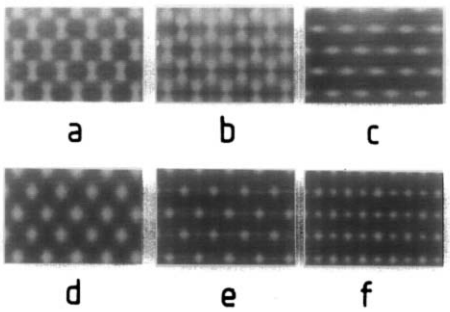


FIG. 2. Computer-simulated images of $LiMn_2O_4$ (a, b, c) and $\lambda$-$MnO_2$ (d, e, f) in the [110] projection. The conditions used were $Cs = 0.52$ mm, objective lens defocus $= -60$ nm, radius of the objective aperture $= 4.0$ nm$^{-1}$, 200 kV. The images are calculated for crystal thicknesses of 2.0 nm (a, d), 4.0 nm (b, e), and 6.0 nm (c, f).

creases still further, the contrast of the double-weight manganese atoms reverses, these then appearing as white dots in both images (Figs. 2c and 2f), but it is clearly evident in the image of λ-$MnO_2$ (Fig. 2f) that a second set of white dots marking the positions of the channel centers still persists. In the image of $LiMn_2O_4$, however, (Fig. 2c), the presence of the lithium atoms, which still scatter with positive (dark) contrast, completely mask the residual white dots at the channel centers. The results from a full multiple scattering calculation therefore confirm the qualitative predictions of the pseudo-weak phase object approximation.

When absolute values of image contrast need to be considered, however, it is necessary to take into account all the factors affecting contrast in addition to the multiple *elastic* scattering referred to above. Of these other factors, the most important are the elastic scattering of initially *inelastically* scattered electrons (*6*), true absorption, and the effects of electron beam misalignment (*10*) both on the multiple scattering process and the resultant image formation. The effects of electron beam tilting within amounts governed by the maximum experimentally measured radius of the divergence disk (ca. $10^{-3}$ rad) and the limits of objective lens alignment were investigated, and although altering the exact form of the contrast in images from both structures, these made no change to the relative differences between images. For example, no matter what degree of beam inclination was employed, it proved impossible to alter the image series from $LiMn_2O_4$ such that it resembled that of λ-$MnO_2$.

For the calculation of effects due to inelastically scattered electrons, the electron energy loss spectra of several crystals were recorded and the absolute energies and areas and full-width half-height maxima of the deconvoluted plasmon loss peaks relative to the zero loss peak were recorded. The data obtained are summarized in Table I. After removal of multiple inelastic scattering by the Fourier-log method of Egerton *et al.* (*11*), an approximate value of the bulk transmission coefficient, $\eta$, in the overall transmission function,

$$\exp(-i\sigma\phi(x, y))\exp(-\eta\phi(x, y)),$$

was derived, the value of $\eta$ finally used in the calculations being 0.00002. Elastic images were then calculated using this transmission coefficient, and allowance was made for images arising from elastic scattering of plasmon loss electrons by simulating the contrast at constant wavelength but slightly different defocus values as discussed above. Although these "inelastic" images showed markedly different contrast to that of the main image, it was found that, for the specimen thicknesses pertaining to the HREM images, the relative contributions of these "inelastic" images was not sufficient to influence the overall image contrast, and had no effect whatsoever on the relative differences between images of $LiMn_2O_4$ and $MnO_2$. Debye–Waller factors were not incorporated into the image simulations, partly because no relevant data were available, but also because in a related study their effect on the overall contrast at 200 kV was found to be minimal (*13*). The results of the simulations therefore were that the marked differences between the

TABLE I

DETAILS OF THE ZERO-LOSS AND PLASMON-LOSS PEAKS IN THE DECONVOLUTED ELECTRON ENERGY LOSS (EELS) SPECTRUM OF $LiMn_2O_4$

| Peak | Energy loss (eV) | FWHM (eV) | Relative weight | Defocus shift (nm) | Focal spread (nm) |
|---|---|---|---|---|---|
| I | 0.0 | 2.0 | 0.622 | 0.0 | 10.5 |
| II | 8.4 | 3.5 | 0.047 | +44.1 | 18.4 |
| III | 24.5 | 20.0 | 0.298 | +128.6 | 105.0 |
| IV | 40.0 | 7.5 | 0.033 | +210.0 | 39.4 |

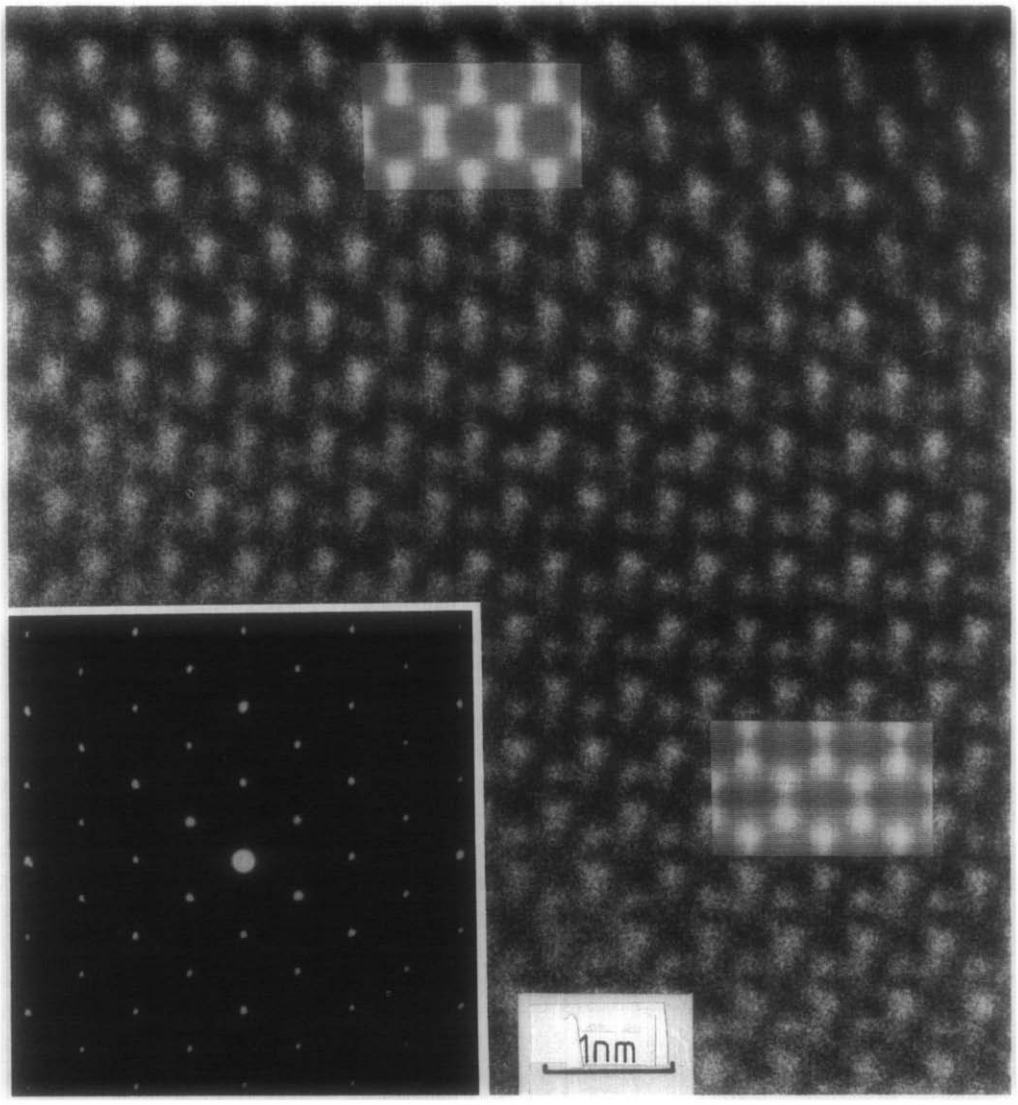


FIG. 3. Experimental HREM image of $LiMn_2O_4$ down [110]. Inset: simulated images correspond to those of Figs. 2a and 2b. The selected area diffraction pattern is also shown.

image contrast in the two materials should be observable experimentally.

Several images in the [110] projection were obtained experimentally from both $LiMn_2O_4$ and $\lambda$-$MnO_2$, these being illustrated in Figs. 3 and 4. Fig. 3 shows one image of $LiMn_2O_4$ where the characteristic splitting of the white dots in the channel centers is very clearly visible, and as shown by the simulated images (inset) computed for thicknesses of 2.0 and 4.0 nm, respectively, the variation of this splitting with increasing specimen thickness closely follows the pattern predicted. This splitting, however, was not observed in images of $\lambda$-$MnO_2$ (Fig. 4) with, as predicted, the white "channels" contracting continually and ultimately being joined in the image by the second set of white dots corresponding to the double-weight manganese atoms with

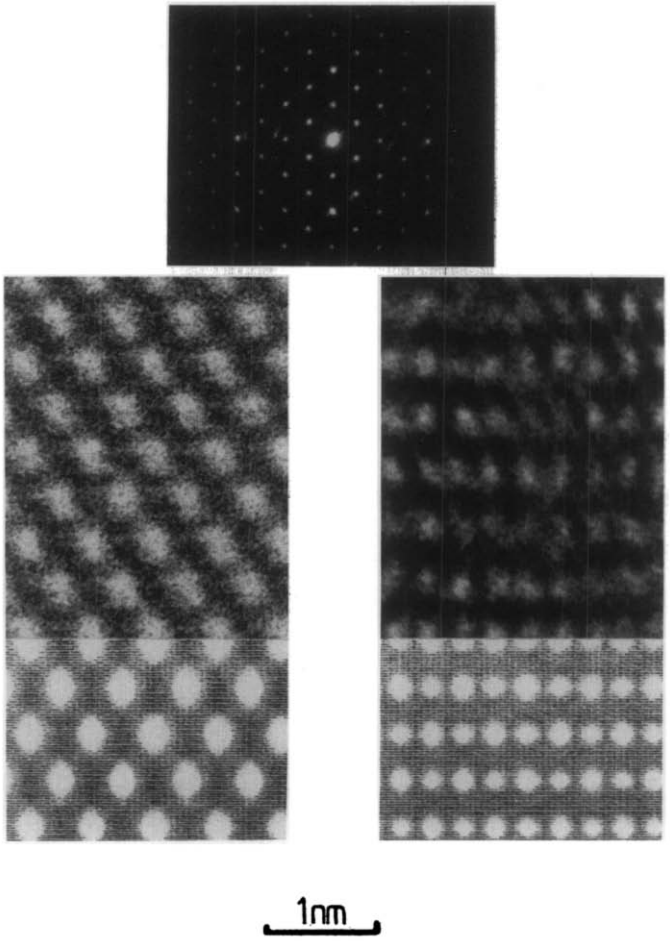


FIG. 4. Experimental HREM images of λ-$MnO_2$ down [110]. Inset: simulated images correspond to those of Figs. 2d and 2f. The selected area diffraction pattern is also shown.

reversed contrast. As most of the crystals examined were of wedge-shaped morphology and therefore showed a noticeable variation of image contrast with specimen thickness (i.e., different contrast at the crystal edge and further into the bulk of the crystal), a clear distinction between the two structures could be made experimentally.

## Conclusions

This study indicates that for specimens of moderate thickness where the contrast from light atoms can be enhanced relative to that of their heavier neighbors by multiple scattering, the presence of such atoms in the structure can be detected by detailed analysis of the observed image contrast, and that for real specimen thicknesses found in finely crystalline materials, the effects due to inelastic processes are insufficient to mask or confuse these differences. Furthermore, if the instrumental resolution can be improved to the point where the very short bond distances between light atoms and their neighbors can be imaged, there appears to be no reason why light atoms should not be revealed as dark dots in the overall contrast. More important however is the fact that the pseudo-weak phase

object approximation appears to hold, at least qualitatively, for specimens of this thickness and potential density, enabling it to be used in a predictive fashion for other, similar structures such as $Li_2Ti_3O_7$ (*3*). In addition, in the specimen thicknesses actually attained in practice the influence of the complications of inelastic scattering is also insignificant.

There are very many solids of particular scientific interest containing lithium for which the previously obtained structural data is scanty and which could benefit from an examination of the type discussed above. For example, transition metal chalcogenides take up lithium and other alkali metals in the process of intercalation, thereby paving the way to the possible production of solid-state batteries. Also, it has been found that many solids of composition $LiMO_2$ or $LiNO_3$, where $M$ and $N$ are appropriate transition metals, are good selective oxidation catalysts, and consequently structural information about the $Li^+$ ions in such phases is a key issue.

## Acknowledgments

D.T. acknowledges the support of the Royal Society for a Queen Elizabeth Fellowship. We are also grateful to The Science and Engineering Research Council for general support and for research studentships to I.J.P. and R.D.B.

## References

1. F. H. Li and D. Tang, *Acta Crystallogr. Sect. A* **41,** 376 (1985).
2. B. M. Gatehouse, P. Goodman, and A. Olsen, *J. Solid State Chem.* **72,** 193 (1988).
3. D. Tang, C. M. Teng, J. Zhou, and F. H. Li, *Acta Crystallogr. Sect. B* **42,** 340 (1986).
4. P. Goodman and A. F. Moodie, *Acta Crystallogr. Sect. A* **30,** 280 (1974).
5. W. M. Stobbs and W. O. Saxton, submitted for publication.
6. D. G. Wickham and W. J. Croft, *J. Phys. Chem. Solids* **7,** 351 (1958).
7. J. C. Hunter, *J. Solid State Chem.* **39,** 142 (1981).
8. D. A. Jefferson, J. M. Thomas, G. R. Millward, K. Tsuno, A. Harriman, and R. D. Brydson, *Nature (London)* **323,** 428 (1986).
9. J. M. Cowley, *Chem. Scr.* **14,** 279 (1979).
10. D. J. Smith, W. O. Saxton, M. A. O'Keefe, G. J. Wood, and M. W. Stobbs, *Ultramicroscopy* **11,** 263 (1983).
11. R. F. Egerton, B. G. Williams, and T. G. Sparrow, *Proc. Soc. London, Ser. A* **398,** 395 (1985).
12. H. P. Erickson and A. Klug, *Philos. Trans. R. Soc. London, Ser. B* **261,** 105 (1971).
13. D. Tang, R. D. Brydson, D. A. Jefferson, and J. M. Thomas, *J. Phys. C.* (in press).